===================== **MATHEMATICAL MODELING** =====================

Computational Analysis of Hysteresis and Bistability in the Mitochondrial Respiratory Chain

Markevich N.I.*[1,2], Hoek J.B.[1]

[1]Department of Pathology, Anatomy, and Cell Biology, Thomas Jefferson University, Philadelphia, PA 19107, USA
[2]Institute of Theoretical and Experimental Biophysics RAS, Pushchino, 142290, Russia

Abstract. Quantitative analysis of bistability in operation of the respiratory chain was performed with the help a computational mechanistic model developed by us earlier. This study included numerical solving of a system of algebraic equations according to steady states in a system of differential equations comprising the computational model and analysis of a wide spectrum of steady-state solutions in the model. Detailed quantitative analysis of the mechanisms of appearance of hysteresis in steady-state characteristics that accords with bistability and conditions of availability of bistability in the entire respiratory chain during oxidation of NADH, succinate and NADH+succinate was carried out. It was shown that although hysteresis and bistability in respiratory chain operation during oxidation of NADH and succinate has the same kinetic mechanism, namely an apparent substrate inhibition of QH_2 oxidation at the Qo-site of Complex III, conditions of bistability arising in respiratory chain fueled by succinate alone differ from those during oxidation of NADH or NADH + succinate because of a different QH_2-dependence of the QH_2 generation rate by Complex II and Complex I. The most important factors which affect occurrence of bistability in the respiratory chain during oxidation of NADH and NADH + succinate are the rates of NADH reduction in the matrix and the total concentration of Complex I [CI] and ubiquinone $[Q]_{tot}$ in the inner membrane. A high rate of NADH reduction and a high ratio $[CI]/[Q]_{tot}$ are condition that would favorable for hysteresis and bistability. The mechanism of a drastic increase in ROS production due to bistable switches in the respiratory chain during hypoxia-reoxygenation suggested earlier by Selivanov and colleagues was analyzed. A computational simulation of hypoxia-reoxygentaion under condition of existence of bistability shows a considerable increase in the rate of ROS production if hypoxia induces a switch of the respiratory chain to the reduced steady state. However, no changes occur in the ROS production rate during reoxygenation following hypoxia compared to the initial state if the membrane potential drops during hypoxia keeping a high rate of respiration and oxidized steady state of the respiratory chain. This implies that additional mechanisms of a considerable increase in ROS production during hypoxia-reoxygentaion which initiate ROS-related cellular hypoxia-reoxygenation injury should be.

Key words: *reactive oxygen species (ROS), mitochondrial respiratory chain, computational model, hysteresis and bistability, hypoxia-reoxygenation.*

---

*markevich.nick@gmail.com

INTRODUCTION

Reactive oxygen species (ROS) generated by mitochondria has been implicated in numerous pathologies and aging [1–3]. Complexes I and III of the mitochondrial respiratory chain are recognized as the important sources of ROS in mammalian cells [4, 5]. Reduction of these complexes due to inhibition of different segments of the respiratory chain can result in a considerable increase in the rate of ROS production [6]. For instance, inhibition of the electron transport chain and accompanying alterations in ROS production during hypoxia, especially, if it is followed by reoxygenation can initiate ROS-related cellular hypoxia-reoxygenation injury [7]. Selivanov and colleagues [8, 9] discovered recently bistability in operation of the respiratory chain and showed computationally that bistability can be a reason of a drastic increase in ROS production during anoxia-reoxygenation. Computational analysis of bistability and an increase in ROS production during anoxia-reoxygenation was made [8, 9] with the help of the rule-based model on the assumption that electron transfer between any redox pair of carriers does not depend on the redox state of the remaining electron carriers in the respiratory chain. Using this simplifying suggestion and describing explicitly the electron transfer between any two transporters that involves a few tens of reactions for the entire respiratory chain, authors were able to develop algorithms (rules) to automatically construct an implicit computational model consisting of a few hundreds differential equations and computing the probability (concentration) of all possible micro-states in Complexes I and III of the respiratory chain. However, this very productive idea to reduce the combinatorial complexity associated with computational models of complex biochemical and biophysical systems, (previously used by our group [10] in the context of cell signaling models) is not necessarily compatible with experimental observations. Experimental observations [11, 12] show that the suggestion of independent interactions in electron transfer is violated in Complex III. For instance, experimental data on the rate of superoxide production by the antimycin A-inhibited Complex III published recently by Brand and coworkers [12] can be accounted for by the assumption that the rate constants of ubiquinol oxidation at the Qo-site strongly depends on the redox state of cyt b. Moreover, the extrinsic domain conformational switch of the iron-sulfur protein (ISP-ED) between the cytochrome b and c_1 positions can also depend on the redox states of cyt bL and bH [11]. In order to take into account changes in the rate constants of electron transfer induced by alterations in the redox state of the respiratory chain, an explicit network computational model is needed, at least for the most important segments of the respiratory chain. How these changes in the rate constants can affect features of the rule-based model of the respiratory chain observed earlier [11, 12], especially, existence of bistability is not understood.

In the present study, we analyze quantitatively the mechanisms of arising of hysteresis in the steady-state characteristics and conditions where hysteresis and bistability exist in operation of the mitochondrial respiratory chain with the help of an explicit network computational mechanistic model of electron transfer and superoxide formation in the respiratory chain which was developed by us earlier [13]. This study aims to find values of rate constants and protein concentration in the model which favorable for bistability in the respiratory chain and check with the help of this model the mechanism of a drastic increase in ROS production during hypoxia-reoxygenation suggested earlier by Selivanov and colleagues [8, 9].

METHODS AND MODELS

1. Kinetic model of mitochondrial respiratory chain

The working kinetic model of the respiratory chain was developed by us earlier [13] with the help of the standard kinetic approach with an explicit graphical representation of the kinetics of electron transfer in the entire respiratory chain (Fig. 1). Reactions (1–40) of the kinetic model in Fig. 1 repeat the same reactions (1–40) from the more extended kinetic model of the respiratory chain taking into account ROS degradation that presented in Fig. 1 of our paper related to ethanol-induced oxidative stress [13]. Detailed justification of this kinetic model, chemical equations and model parameters are presented in Tables 1, 2 from the paper [13].
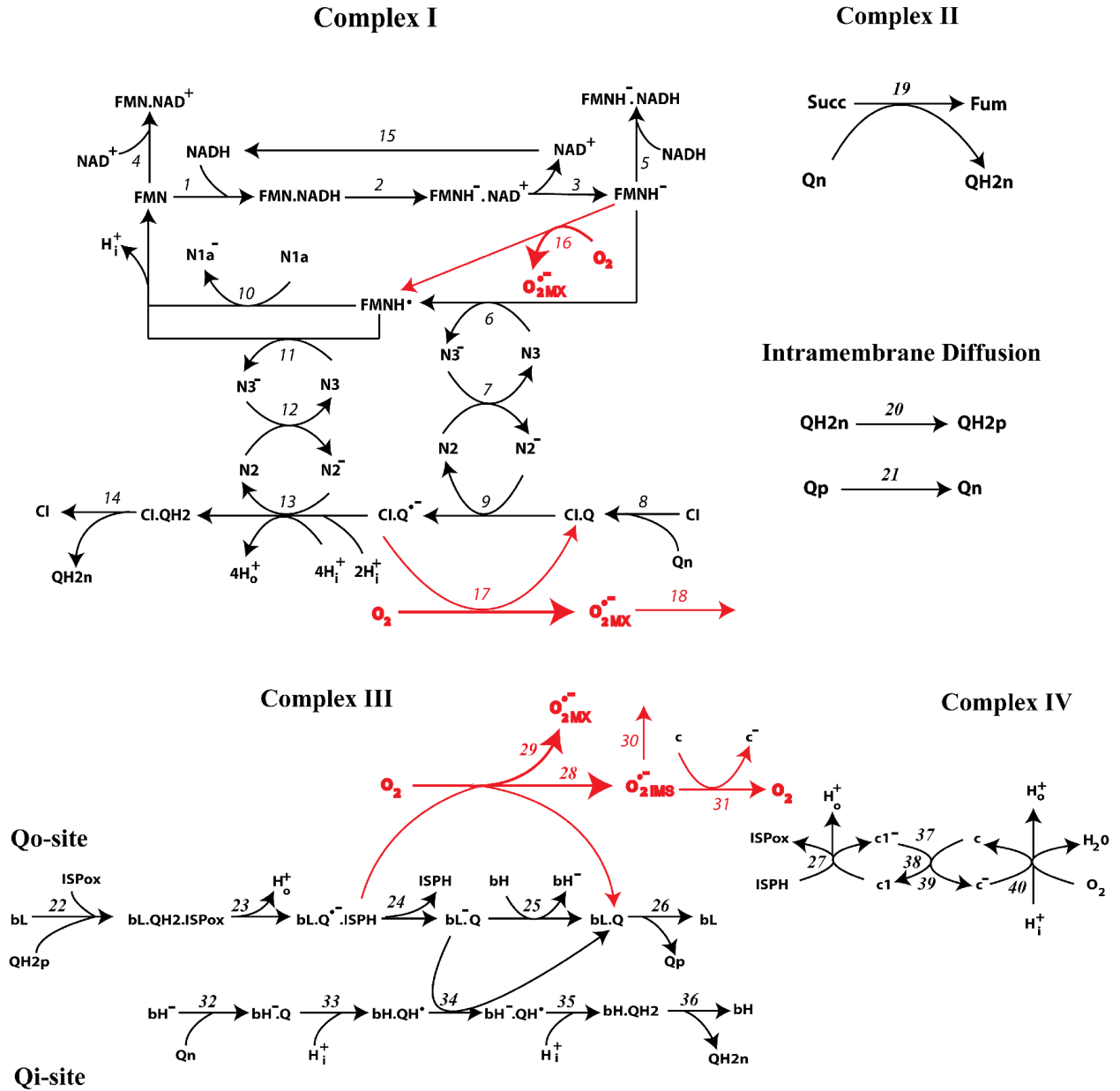

Figure 1. Kinetic scheme of electron transfer and superoxide production in the respiratory chain with early dissociation of ISPH in complex III. Reactions of ROS formation and utilization are shown by red arrows. Detailed reaction network is presented in Table 1 from our earlier paper [13].

91

A kinetic scheme of electron transfer and superoxide anion production underlying a mechanistic computational model of the mitochondrial respiratory chain (Fig. 1) includes the following electron carriers: a) for Complex I (NADH dehydrogenase, also called NADH:Ubiquinone Oxidoreductase), flavine mononucleotide (FMN), the sequence of iron-sulfur clusters beginning N3 and N1a and ending N2 cluster, and coenzyme Q; b) for Complex III (Cytochrome bc1 complex, also called Ubiquinol:Cytochrome c Oxidoreductase), coenzyme Q, non-heme iron-sulfur protein (ISP), cytochromes bL, bH and c1; c) Cytochrome c and d) Cytochrome c oxidase, also known as Complex IV. Complex II (Succinate dehydrogenase) and Complex IV are taken as the total complexes, since Complexes II and IV are not direct sources of ROS during mitochondrial electron transport. Electron transfer in Complexes I and III were described in detail to take into account electron carrier states responsible for bypass reduction of O_2 resulting in superoxide formation. These bypass reactions are marked by red arrows in the kinetic scheme (Fig. 1). The entire reaction network of electron transfer and superoxide production corresponding to this kinetic scheme in Fig. 1 consists of 40 reaction rates which are described in detail in Table 1 from our earlier paper [13].

Our current explicit network kinetic model of the respiratory chain differs from the rule-based model developed recently by Selivanov and colleagues [8, 9] on the assumption that electron transfer between any redox pair of carriers does not depend on the redox state of the remaining electron carriers in the respiratory chain. In our model, rate constants of electron transfer between any transporters can depend on the redox state of the respiratory chain.

However, it should be pointed out that a difference in the rule-based model and our current model is not as dramatic as it may appear at first glance. In reality, all states of the respiratory chain presented in the explicit network kinetic model (Fig. 1) are macro-states that correspond to experimentally verifiable variables and involve a sum of numerous micro-states of the respiratory chain. For instance, any macro-state in Complex III, e.g. oxidized cyt bL includes the sum of all possible micro-states, reduced and oxidized, of Complex I. This implies that the explicit network kinetic model is developed at least in part on the assumption of independence of molecular events occurring at distinct electron carriers, as does the rule-based model.

2. Computational model of electron transfer in mitochondrial respiratory chain

A computational model consisting of 32 ordinary differential equations (ODE) and 12 moiety conservation equations was derived from the reaction network using the law of mass action, Michaelis and Hill kinetics for all 40 kinetic processes. All equations are presented in Appendix. The model was implemented in DBSolve Optimum software available at website http://insysbio.ru. Numerical integration of model equations has been performed with *ODEs solver* of DBSolve while system of algebraic equation according to steady-state solutions in the model was solved with *Implicit solver* of DBSolve. Values of model parameters, rate constants and concentration of different electron carriers, were taken from literature experimental data on thermodynamics and kinetics of electron transfer in respiratory chain and presented in Table 2 from [13].

RESULTS AND DISCUSSION

1. Hysteresis and bistability in the kinetics of electron transfer in the respiratory chain

1.1. Hysteresis and bistability are intrinsic features of the respiratory chain

Selivanov and colleagues [8] analyzing anoxia-induced ROS production in the respiratory chain fueled by succinate alone discovered computationally and proved experimentally the

92

existence of two steady-state modes (bistability) of operation of Complex III. They confirmed recently [9] availability of bistability in operation of the respiratory chain during oxidation of NADH-linked substrates with the help of the rule-based model. Computational analysis of bistability in the rule-based model [8, 9] was made with numerical integration of model equations. In the present study, analyzing hysteresis and bistability in the respiratory chain we solve directly a system of algebraic equations according to steady states in a system of differential equations comprising the computational model developed by us earlier [13] and analyze a wide spectrum of steady-state solutions in the model. First of all, we analyze quantitatively the mechanism of appearance of hysteresis in steady-state characteristics and conditions of availability of bistability in the entire respiratory chain with the help of the explicit network computational model.
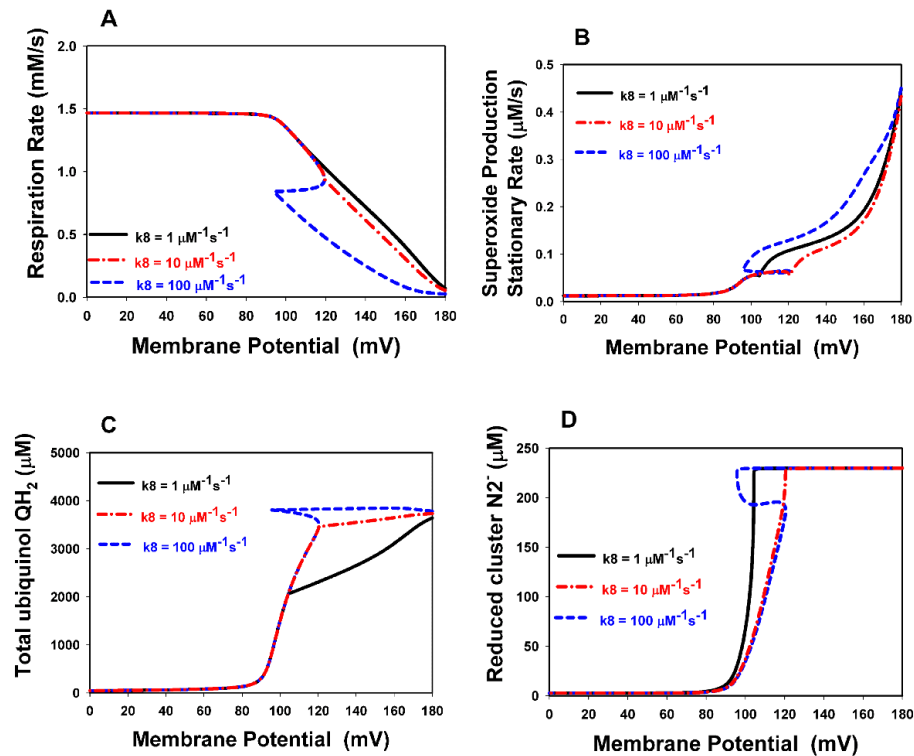

Figure 2. Hysteresis and bistability appearance in the dependence of steady state characteristics of the respiratory chain on the membrane potential at increasing the rate constant (k_8) of Q binding to Complex I. Computer simulated membrane potential dependence of steady state: (**A**) the respiration rate; (**B**) the total ROS generation rate; (**C**) a membrane pool of ubiquinol QH_2; (**D**) reduced Fe-S claster N2. Computer simulation was carried out with the mathematical model at kinetic parameter values presented in Table 2 [13] except k_8, which are shown in the Figure. Black solid curves correspond to $k_8 = 1$ $\mu M^{-1}s^{-1}$; red dash-dot curves – $k_8 = 10$ $\mu M^{-1}s^{-1}$; blue dashed curves – $k_8 = 100$ $\mu M^{-1}s^{-1}$. NADH + succinate were simulated as respiratory substrates. $V_{max19} = 4270$ $\mu M \cdot s^{-1}$; $k_{15} = 0.45$ s^{-1}.

The kinetic parameter values related to our basic model are presented in Table 2 [13]. These values were adjusted to account for experimental observations of ROS production in liver mitochondria [14]. However, a comparison of results on ROS production from a selection of studies on isolated mitochondria from different tissues shows a very high degree of variability in the ROS production rate [15]. Therefore, we assume that some rate constants and protein concentration in the model can depend on experimental conditions and tissues. First of all, this relates to the rate constants of binding Q and QH_2 to Complexes I and III. Our computational modeling analysis revealed that simulation of changes in the Q and QH_2 binding constant to

93

Complex I can bring about qualitatively such important features as bistability [8, 9] in the kinetics of electron transfer and ROS production in the respiratory chain during oxidation of different substrates. In particular, we analyzed hysteresis and bistability in operation of the respiratory chain during oxidation of NADH alone or NADH + succinate.

Fig. 2 shows that a computer simulated increase in the rate constant k_8 of Q association with Complex I (reaction (8) in Fig. 1 and Table 1 from [13]) from 1 to 100 $\mu M^{-1}s^{-1}$ results in hysteresis in the membrane potential dependence of the steady-state respiration rate (Fig. 2,A) and the ROS generation rate (Fig. 2,B), as well as a membrane pool of ubiquinol QH_2 (Fig. 2,C) and reduced Fe-S claster N2 (Fig. 2,D). It should be noted that hysteresis and bistability in the stationary dependence of the redox state of the respiratory chain on the membrane potential is computationally observed for all electron carriers of Complexes I and III. The computer simulated results presented in Fig. 2 were obtained with NADH + succinate as respiratory substrates.

The mechanism to account for hysteresis and bistability in electron flow and redox state of different electron carriers presented in Fig. 2 is purely kinetic nature and as was noticed earlier [8] results from the conservation relationship between oxidized and reduced pools of ubiquinone (Q and QH_2) in the inner membrane.
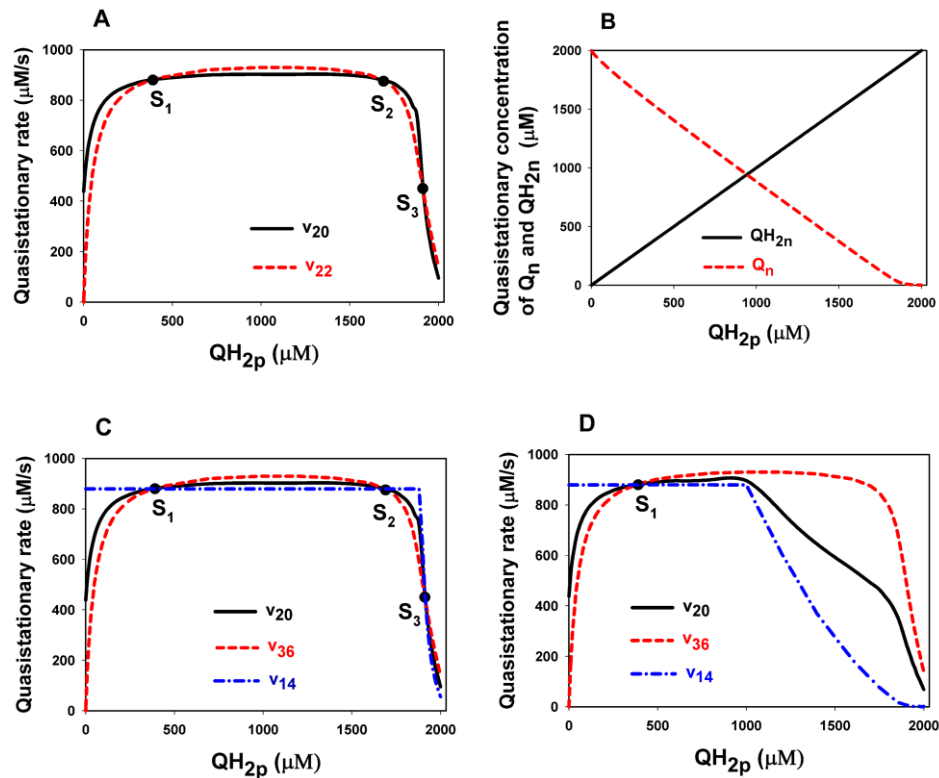

Figure 3. Dependence of quasi-stationary rates and QH2n and Qn on QH2p during oxidation of NADH alone. Three intersections point S1, S2, and S3 correspond to three steady states in the model (A, C). S2 is unstable and S1, S3 are stable steady states. Computer simulation was carried out with NADH alone as fuel substrate. $\Delta\Psi$ =130 mV. All parameter values are the same as in Fig. 2 except $k_8 = 100$ $\mu M^{-1}s^{-1}$ (A–C) and $k_8=1\mu M^{-1}s^{-1}$ (D). See text for detail.

Fig. 3 explains graphically how bistability arises in the mathematical model presented above. We analyzed so called quasi-stationary characteristics, proposing that one variable QH2p, concentration of ubiquinol at cytoplasmic (positive) side of the inner membrane, in the model is

fixed at some value, and remaining variables take the steady state values, which correspond to the value of the fixed variable. We solved the system of ODE presented in Appendix at following conditions: QH2p = const, which runs all values presented in Fig. 3, and $F[i] = 0$, where $i = 2, \ldots, 32$.

Computational simulation analysis shows (Fig. 3,A) that a dependence of the quasi-stationary rate of QH2p consumption (v_{22}) on QH2p has the bell-shaped form like a biochemical reaction with substrate inhibition. Unusual falling down of v_{22} at high QH2p values occurs due to a depletion of Qn, concentration of ubiquinone at matrix (negative) side of the inner membrane, at increasing QH2p (Fig. 3,B). A depletion of Qn at high QH2p results from only the ubiquinone total pool conservation. Deficiency of Qn results in inhibition of the rate of reactions at the Qi-site (reactions 32–36) and reactions (22–26) at the Qo-site since all rates of consecutive electron transfer in the Q-cycle are equal at steady state. This apparent substrate inhibition can bring about three alternative steady states in the model which satisfy to the stationary condition $F[1] = v_{20} - v_{22} = 0$. i. e. equality quasi-stationary rates of generation (v_{20}) and consumption (v_{22}) QH2p. Fig. 3,A shows that three intersections of curves v_{20} and v_{22}, designated S_1, S_2, and S_3, which correspond to two alternative stable steady states (S1 and S3) and one unstable state (S2) may be in the model during oxidation of NADH alone. One can see that for bistability to arise the curve v_{20} has to fall down at high QH2p steeper than v_{22}. This condition is satisfied at high values of the rate constant of Qn association with Complex I, k_8, for the following reason. The quasi-stationary rate $v_{20} = k_{20} \cdot (QH2n - QH2p)$ follows the rates of QH2n generation by Complex I, v_{14}, and the Qi-site of Complex III, v_{36}, because of steady state condition for QH2n in the system of ODE presented above, $F[2] = v_{19} - 2 \cdot v_{20} + v_{36} + v_{14} = 0$. That is $v_{20} = (v_{14} + v_{36})/2$ since $v_{19} = 0$ during oxidation of NADH alone. Fig. 3,C shows that dependence of the quasi-stationary rate v_{20} on QH2p locates between the rates v_{14}, and v_{36}. As we mentioned above $v_{36} = v_{22}$ at steady state condition in the Q-cycle, so, for bistability to arise v_{20} should fall down steeper than v_{36} that could be only at steepness of falling down of v_{14} more than v_{36} or, in other words, v_{14} should increase at increasing Qn steeper than v_{36} due to inverse relationship between QH2p and Qn that could be at high values of the rate constant of Qn association with Complex I, k_8. Fig. 3,D shows that a decrease in k_8 results in slow falling down of v_{14} and v_{20} at increasing QH2p and disappearing two steady states, S2 and S3, i.e. disappearing bistability.
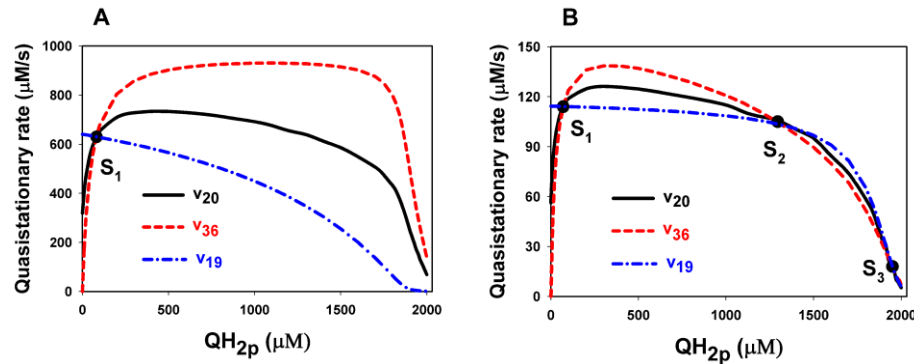

Figure 4. Dependence of quasi-stationary rates v_1, v_{20}, and v_{36} in the model during oxidation of succinate alone. (A) All parameter values are the same as in Fig 3. $\Delta\Psi = 130$ mV. (B) All parameter values are the same as in Fig 3 except $K_{19} = 0.05$; $V_{max19} = 500$ μM/s; $k_{26} = 5\cdot10^3$ s^{-1}; $k_{32} = 0.02$ μM^{-1}s^{-1}. $\Delta\Psi = 140$ mV. Three intersections point S1, S2, and S3 correspond to three steady states in the model. S2 is unstable and S1, S3 are stable steady states. Computer simulation was carried out with succinate alone as fuel substrate.
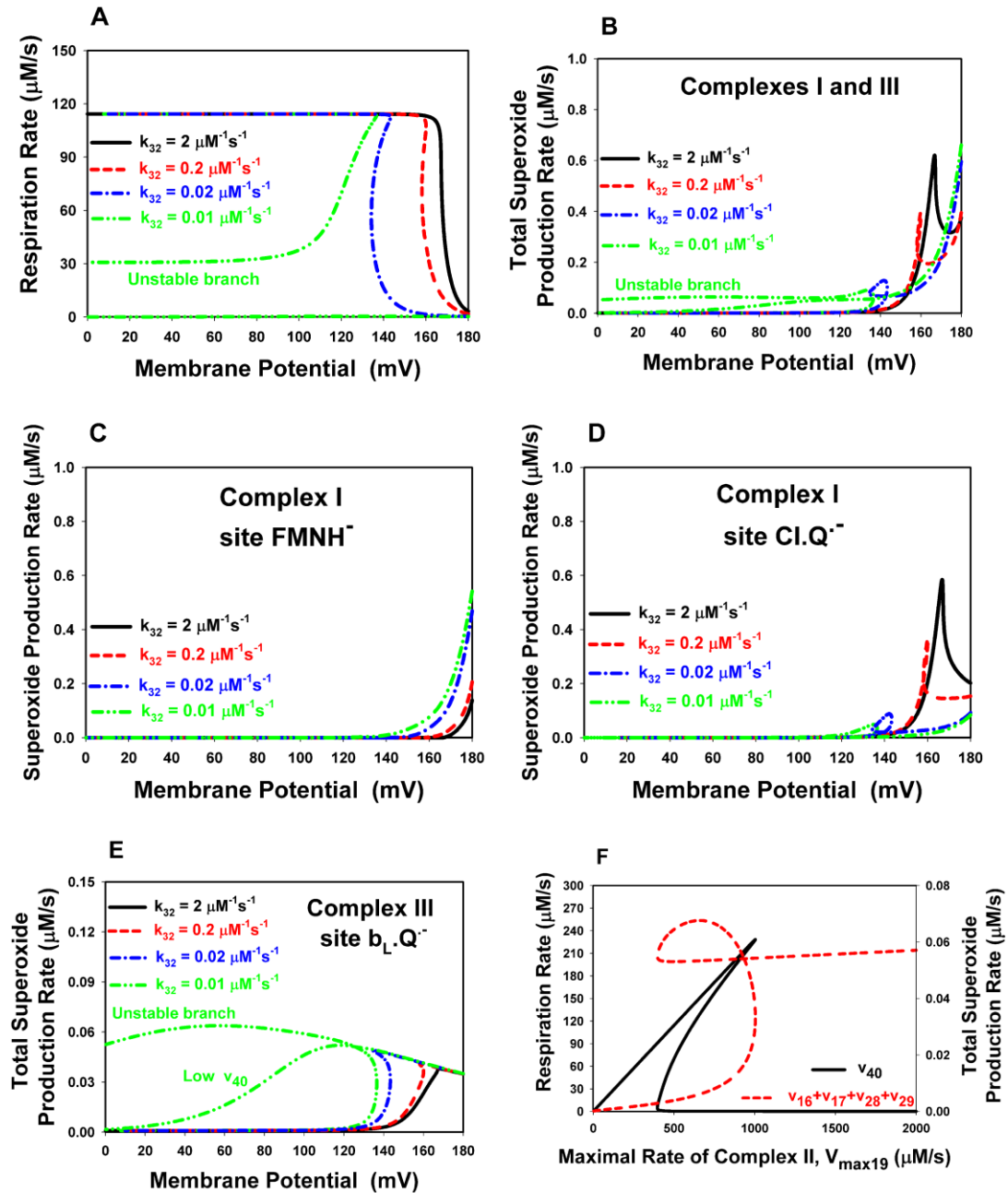
Figure 5. Hysteresis and bistability appearance in operation of the respiratory chain during oxidation of succinate alone at a decrease in the rate constant (k_{32}) of Q binding to the Qi-site of Complex III. **(A–E)** A dependence of the stationary rates of respiration and superoxide production on membrane potential at different values of k_{32}. **(A)** The respiration rate. **(B)** The total rate of ROS production by Complexes I and III. **(C–E)** The rate of ROS generation by different sites of Complexes I and III: **(C)** site FMNH⁻ of Complex I; **(D)** semiquinone of Complex I (site CI.Q⁻); **(E)** unstable semiquinone of Complex III (site bL.Q⁻). **(F)** The stationary rate of respiration (black solid curve) and total ROS production by Complexes I and III (red dashed curve) at ΔΨ=130 mV and different values of the maximal rate of succinate dehydrogenase (Complex II), V_{max19}. Computer simulation was carried out at all parameter values the same as in Fig. 3 in the main text except $K_{19} = 0.05$, $V_{max19} = 500$ μM/s, $k_{26} = 5\cdot10^3$ s⁻¹, and, k_{32} which are shown in Figs (A–E) and $k_{32} = 0.02$ μM⁻¹s⁻¹ for (F). **(A–E)** Black solid curve corresponds to $k_{32} = 2$ μM⁻¹s⁻¹; red dashed curve – $k_{32} = 0.2$ μM⁻¹s⁻¹; blue dash-dot curve – $k_{32} = 0.02$ μM⁻¹s⁻¹; green dash-dot-dot curve – $k_{32} = 0.01$ μM⁻¹s⁻¹.

By analogy, Fig. 4 presents quasi-stationary rates in the model during oxidation of succinate alone. In this case, the rate $v_{20} = (v_{19} + v_{36})/2$ because of $v_{14} = 0$ (no NADH). Fig. 4,A shows that our basic model has only one stable steady state at succinate alone as respiratory substrate due to slower falling down of v_{19} and, accordingly, v_{20} than $v_{36} = v_{22}$ at increasing QH2p. It results from high values of dimensionless Michaelis constant K_{19} ($K_{19} = 0.6$) for succinate dehydrogenase and the rate constant k_{32} of Qn association with the Qi-site and k_{26} of Qp dissociation from the Qo-site of Complex III (Table 2 in [13]). A decrease in K_{19}, k_{26} and k_{32} results in appearance of three intersections of curves v_{20} and v_{36} (v_{22}) designated as S_1, S_2, and S_3 (Fig. 4,B) which accord with three steady states and hysteresis in the model during oxidation of succinate alone presented in Fig. 5.

Thus, we showed that bistability arises in the respiratory chain during oxidation of NADH alone (Fig. 3) because of a dependence of the quasi-stationary rate of QH2p consumption (v_{22}) on QH2p has a bell-shaped form, similar to a biochemical reaction with substrate inhibition. Substrate (succinate) inhibition of electron flow in Complex III at high succinate concentration was observed earlier [8] and explained by authors by a deficiency of Q at high concentration of QH_2 due to mass conservation. According to [8] explanation a deficiency of oxidized Q results in inhibition of reoxidation of cyt bH at the Qi-site and, as a result, inhibition of the rate of respiration. Essentially the same argument of deficiency of Qn at high concentration of QH2p resulting in inhibition of electron flow at the Qi-site can explain an apparent substrate inhibition of the quasistationary rate of QH2p consumption in our model during NADH oxidation.

Substrate inhibition in biochemical reactions can result in bistability in metabolic pathways [16]. However, it is not a sufficient condition for bistability to arise. A steady state in the model occurs when the quasistationary rate of QH2p consumption (v_{22}) is equal to the quasistationary rate of QH2p generation (v_{20}). Therefore, hysteresis and bistability arising in the operation of the respiratory chain also depend on features of the rate of QH2p generation, which are different during NADH and succinate oxidation, i.e., for Complexes I and II generating QH_2 (Fig. 3 and Fig. 4). Our computer simulation analysis shows that association of Q with Complex I should be fast for bistability to arise in the respiratory chain during NADH or NADH + succinate oxidation (Fig. 2). The fast Q association rate with Complex I results in a steep increase in the rate of QH_2 generation by Complex I (v_{14}) with an increase in Q and, accordingly, a steep drop of v_{14} at increasing QH_2 which is very important for three alternative steady states and bistability to arise in respiratory chain at NADH oxidation (Fig. 3).

Absolute values of the rate constant of association of Q with Complex I (k_8) are unknown although they may be estimated taking into account the catalytic constant of Complex I. Complex I is not rate-limiting during NADH oxidation by the respiratory chain, because the iron-sulphur clusters of Complex I are almost completely reduced during steady-state aerobic NADH oxidation [17]. The turnover number of Complex I is around 150–200 s^{-1} in bovine heart mitochondria [17] and it may be so high as 600 s^{-1} as reported for *E. coli* [18, 19], so, the second-order rate constant of association of Q with Complex I is really very high and favorable for hysteresis to arise. Thus, we found that the rate constant k_8 of Q association with Complex I very important intrinsic parameter for bistability to arise during oxidation of NADH and NADH + succinate.
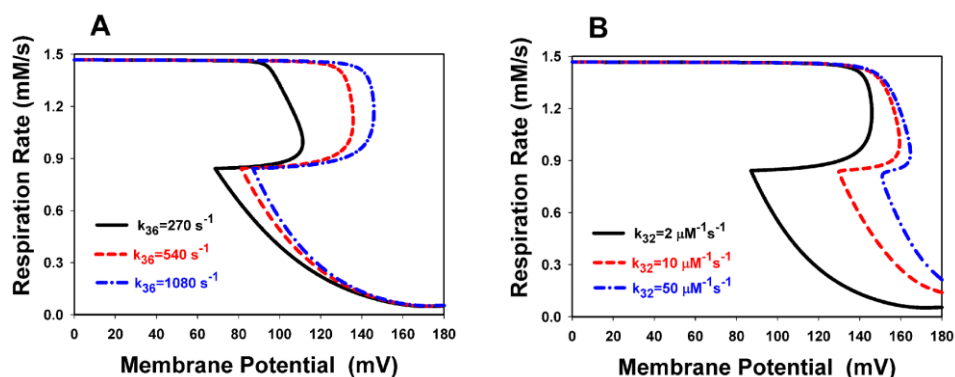
97

Figure 6. A shift of hysteresis in the respiration rate to more positive values of the membrane potential at an increase in the rate constants of Q binding to the Qi-site (k_{32}) and QH$_2$ dissociation from the Qi-site (k_{36}). All parameter values at computer simulations are the same as for Fig. 2 except $k_8 = 100$ μM^{-1}s^{-1}. Values of k_{32} and k_{36} are shown in the Figure. (**A**) $k_{32} = 2$ μM^{-1}s^{-1}. Black solid curve corresponds to $k_{36} = 270$ s^{-1}; red dashed curve – to $k_{36} = 540$ s^{-1}; blue dash-dot curve $k_{36} = 1080$ s^{-1}. (**B**) $k_{36} = 1000$ s^{-1}. Black solid curve corresponds to $k_{32} = 2$ μM^{-1}s^{-1}; red dashed curve – $k_{32} = 10$ μM^{-1}s^{-1}; blue dash-dot curve – $k_{32} = 50$ μM^{-1}s^{-1}. NADH + succinate were simulated as respiratory substrates.

The most important intrinsic parameters which affect hysteresis and bistability in the respiratory chain are the rate constants of binding Q and QH$_2$ to Complex III. Fig. 6 shows that an increase in the rate constants k_{32} and k_{36} of association of Q with the Qi-site and dissociation of QH$_2$ from the Qi-site, respectively, results in a shift of hysteresis to more positive the membrane potential. Herewith, increasing k_{36} (Fig. 6,A) extents hysteresis, while an increase in k_{32} (Fig. 6,B) diminishes the region of existence of hysteresis. It should note that equilibrium constants K_{eq32} and K_{eq36} were kept unchanged in these computer simulations. That means that rate constants k_{-32} and k_{-36} increase with increasing k_{32} and k_{36}, respectively.

1.2. Extrinsic parameters controlling hysteresis and bistability in the respiratory chain

The most important factors that may affect bistability in the respiratory chain and can be controlled experimentally are the rates of supply of Complexes I and III by substrates NADH and QH$_2$, respectively. Fig. 7 presents computer simulated rates of respiration and total ROS generation by Complexes I and III at different values of the rate constant k_{15} which represents the rate of NAD$^+$ reduction to NADH in mitochondrial matrix (Fig. 7,A and 7,B) and V_{max19}, the maximal rate of succinate dehydrogenase (Complex II), which affects the rate of Q reduction to QH$_2$ by Complex II (Fig. 7,C and 7,D). Fig. 7,A and 7,B shows that hysteresis in the steady-state rates of respiration and ROS production disappears at low values of k_{15}, when succinate becomes the main fuel for respiratory chain. This is compatible with the results presented in Fig. 2, which show that hysteresis arises at a high rate of forward electron transfer in Complex I.

Fig. 7,C and 7,D presents computer simulated steady-state rates of respiration and total ROS generation by Complexes I and III at different values of V_{max19}. It can be seen that availability of hysteresis in the respiration and ROS production rates is a little affected by the activity (V_{max19}) of Complex II during oxidation of NADH+succinate at a high rate of NADH supply, i.e. a high value of k_{15}. This result clearly shows that hysteresis arises from forward electron transfer in Complex I at NADH oxidation and any increase in reverse electron transfer results in a little disappearing of hysteresis.
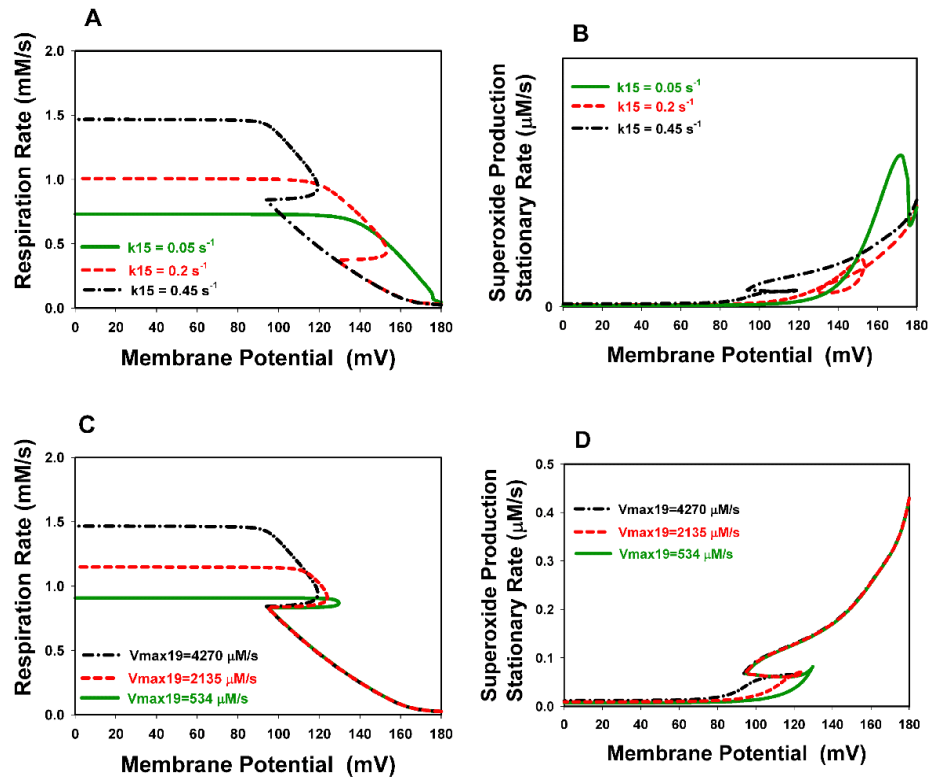
98

Figure 7. Computer simulated rates of respiration and ROS formation at different activity of NADH regeneration and succinate dehydrogenase. (**A, B**) Simulated stationary rates of respiration (A) and total ROS production (B) at different values of k_{15} which represents the rate of NAD$^+$ reduction to NADH in mitochondrial matrix. Solid green curve corresponds to $k_{15} = 0.05$ s^{-1}; red dashed curve – $k_{15} = 0.2$ s^{-1}; black dash-dot curve – $k_{15} = 0.45$ s^{-1}. (**C, D**) Simulated stationary rates of respiration (C) and total ROS production (D) at different values of V_{max19}, maximal rate of succinate dehydrogenase (Complex II). Solid green curve corresponds to $V_{max19} = 534$ μM·s^{-1}; red dashed curve – $V_{max19} = 2135$ μM·s^{-1}; black dash-dot curve – $V_{max19} = 4270$ μM·s^{-1}. Computer simulation was carried out with NADH + succinate as respiratory substrates. Values of k_{15} and V_{max19} are also shown in Figs. (**A, B**) and (**C, D**), respectively. The rest parameter values are the same as for Fig. 2.

Other parameters that have significant effect on hysteresis and ROS production are the concentration of Complex I and ubiquinone in the inner membrane. Fig. 8 presents computer simulated steady-state rates of respiration and total ROS generation by Complexes I and III at different values of concentration of Complex I, [CI] (Fig. 8,A and 8,B) and total Q, [Q]$_{tot}$ (Fig. 8,C and 8,D) in the inner membrane. One can see that 2-, 4-, 8-fold increase in [CI] results in almost same extension in hysteresis as 2-, 4-, 8-fold decrease in [Q]$_{tot}$. Thus, the real parameter controlling hysteresis under conditions of NADH+succinate oxidation is the ratio [CI]/[Q]$_{tot}$. Hysteresis disappears at low values of [CI]/[Q]$_{tot}$ (around 0.01) and becomes extremely extended at [CI]/[Q]$_{tot} > 0.1$.

1.3. Bistability during oxidation of succinate alone

Some specific computer simulated features of bistability in operation of the respiratory chain during oxidation of succinate alone that were discovered earlier by Selivanov and colleagues [8] are presented in Appendix (Fig. 4 and Fig. 5). Conditions of bistability arising in respiratory chain with oxidation of succinate alone differ from those mentioned above during NADH or NADH + succinate oxidation because of a different QH$_2$-dependence of the QH$_2$ generation rate by Complex II (v_{19}) and Complex I (v_{14}).
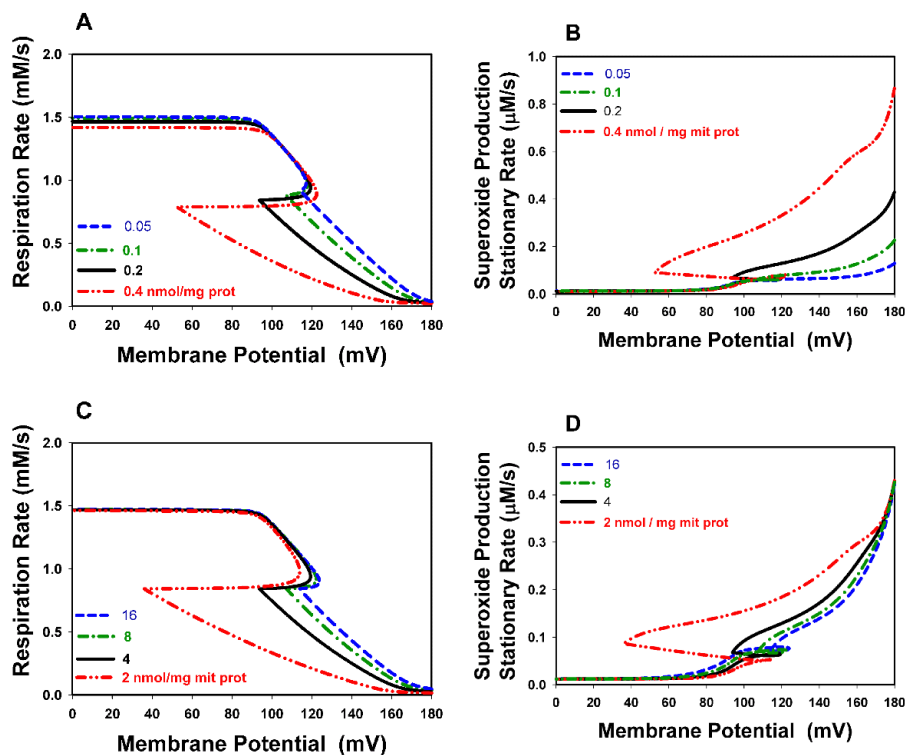
Figure 8. Computer simulated rates of respiration and ROS generation at different content of Complex I and total ubiquinone in inner mitochondrial membrane. (**A, B**) The computer simulated rate of respiration (A) and total ROS production by Complexes I and III (B) at changes in Complex I content measured in nmol/mg mit.prot. Blue dashed curve corresponds to Complex I content [CI] = 0.05; green dash-dot curve – [CI] = 0.1; black solid curve – [CI] = 0.2; red dash-dot-dot curve – [CI] = 0.4. (**C, D**) The computer simulated rate of respiration (C) and total ROS production by Complexes I and III (D) at changes in total ubiquinone content in the inner membrane measured in nmol/mg mit.prot. Blue dashed curve corresponds to total ubiquinone content $[Q]_{tot} = 16$; green dash-dot curve – $[Q]_{tot} = 8$; black solid curve – $[Q]_{tot} = 4$; red dash-dot-dot curve – $[Q]_{tot} = 2$. Values of all parameters are the same as for Fig. 2 except Complex I and total ubiquinone content in the inner membrane. [CI] = 0.2 nmol/mg mit.prot. and $[Q]_{tot} = 4$ nmol/mg mit.prot. in the base model.

Computer simulation analysis shows that our basic model has only one stable steady state (no bistability) with succinate alone as respiratory substrate due to slow decline of v_{19} with increasing QH_2 (Fig. 4,A). This results from the experimentally observed a high value of the dimensionless Michaelis constant K_{19} ($K_{19} = 0.6$) for succinate dehydrogenase [20] and high rate constants k_{32} of Qn association with the Qi-site and k_{26} of Qp dissociation from the Qo-site of Complex III (see Table 2 in [13]). However, a decrease in K_{19}, k_{26} and k_{32} can result in the appearance of three alternative steady states (Fig. 4,B) and hysteresis and bistability in the model during oxidation of succinate alone (Fig. 5). Experimental observations of bistability in the ROS production rate during oxidation of succinate alone [8] predict that K_{19} should be less than the apparent K_m value for exogenous ubiquinone-2 measured experimentally in [19] and, in reality, as was noted earlier [8] kinetic parameters of succinate oxidation (K_{19} and V_{max19}) in Complex II could depend on succinate transport.

2. Computer simulated ROS production during hypoxia-reoxygenation

Selivanov and colleagues [8] proposed that bistability in operation of Complex III during oxidation of succinate alone can underlie anoxia-induced ROS production. They showed computationally that temporal anoxia can switch the respiration rate from the high steady state with a low ROS production to the steady state with a low respiration and a high ROS production,

100

which can persists after returning oxygen to the normal concentration. In this study, alterations in the ROS production rate during hypoxia-reoxygenation were analyzed in more detail with our explicit computational model under hysteresis and bistability conditions in the respiratory chain during oxidation of NADH + succinate.

The oxygen concentration is one of the most important extrinsic parameters which affect superoxide generation in the respiratory chain. Experimental observations of the dependence of mitochondrial ROS generation on the oxygen concentration are controversial [21–23]. Some of the observations [21] show that hypoxia induces ROS production, while other [23] are consistent with the proportional dependence of the ROS production rate on the oxygen concentration. We analyzed oxygen sensitivity of ROS production in the respiratory chain with our computational model that allows us to exclude any external sources of ROS. Hypoxia has two opposite effects on the rate of superoxide generation in the respiratory chain. First of all, oxygen is the substrate in the reactions (16, 17, 28, 29) of the superoxide generation, therefore, a decrease in the oxygen concentration should decrease the overall superoxide production rate. On the other hand, hypoxia results in inhibition of the respiration rate and a reduction of electron carriers that favorable for superoxide generation. Fig. 9,A and 9,B presents a steady-state membrane potential dependency of the rates of respiration (Fig. 9,A) and overall superoxide generation by Complexes I and III (Fig. 9,B) during oxidation of NADH + succinate at different oxygen concentration.
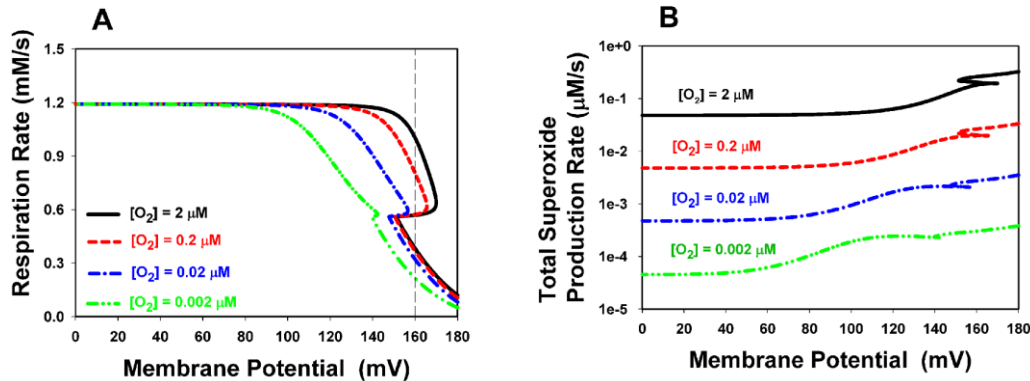

Figure 9. Oxygen sensitivity of steady-state rates of respiration and ROS production. (**A, B**) Computer simulated steady-state dependence of the rates of respiration (A) and total superoxide production (B) on the membrane potential at different oxygen concentration, $[O_2]$. Black solid curves correspond to $[O_2] = 2$ μM; red dashed curves – $[O_2] = 0.2$ μM; blue dash-dot curves – $[O_2] = 0.02$ μM; green dash-dot-dot curves – $[O_2] = 0.002$ μM. All parameter values at computer simulations are the same as for Fig. 2 except $k_8 = 100$ μM^{-1}s^{-1}; $k_{28} = 10$ μM^{-1}s^{-1}; $k_{29} = 10$ μM^{-1}s^{-1}; $k_{32} = 20$ μM^{-1}s^{-1}; $k_{36} = 1000$ s^{-1}. NADH + succinate were simulated as respiratory substrates. $V_{max19} = 4270$ μM·s^{-1}; $k_{15} = 0.45$ s^{-1}.

These steady-state characteristics have a hysteresis shape and were obtained under conditions of existence of bistability for using them at a further analysis of bistable switches in ROS producton during hypoxia-reoxygenation. Our computer simulated results show (Fig. 9,B) that the overall steady-state rate of superoxide generation decreases with decreasing oxygen concentration at any membrane potential, i.e. at any metabolic state of mitochondria. These data are compatible with experimental observations [23] of proportional relationship between the ROS production rate and oxygen concentration.
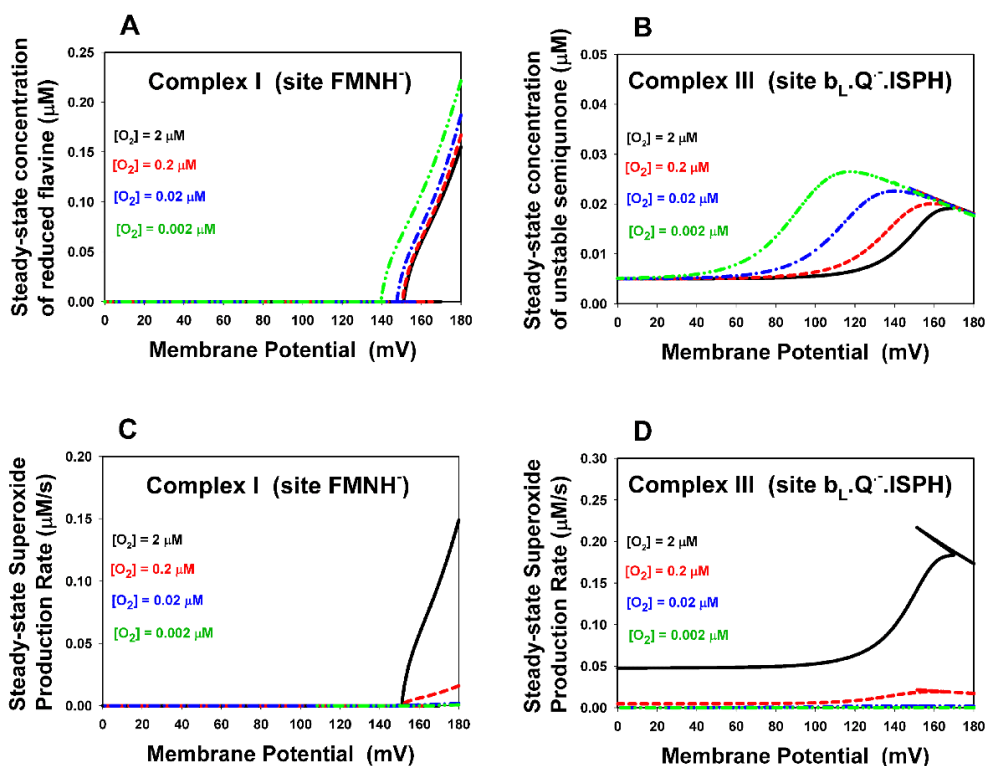
101

Figure 10. A dependence of steady-state kinetic characteristics of reduced flavin in Complex I and unstable semiquinone in Complex III on the oxygen concentration. (**A–D**) Steady-state concentrations of ROS-generaring sites, reduced flavin (FMNH⁻) in Complex I (A) and the unstable semiquinone (complex $b_L.Q^-$.ISPH) in Complex III (B), and rates of superoxide production by these sites, FMNH⁻ (C) and $b_L.Q^-$.ISPH (D) at different oxygen concentration, $[O_2]$. Black solid curves correspond to $[O_2] = 2$ μM; red dashed curves – $[O_2] = 0.2$ μM; blue dash-dot curves – $[O_2] = 0.02$ μM; green dash-dot-dot curves – $[O_2] = 0.002$ μM. All parameter values at computer simulations are the same as for Fig. 6. NADH + succinate were simulated as respiratory substrates ($V_{max19} = 4270$ μM·s⁻¹; $k_{15} = 0.45$ s⁻¹).

Fig. 10 illustrates that, although concentration of superoxide-generating sites, the reduced flavin in Complex I (Fig. 10,A) and the unstable semiquinone in Complex III (Fig. 10,B), increase with a decrease in the oxygen concentration, the rates of ROS production by these sites decreases during hypoxia (Fig. 10,C and 10,D).

The other conclusion resulted from Fig. 9,A and 9,B is shifting of hysteresis in the rates of respiration and ROS production to a low values of the membrane potential with decreasing the oxygen concentration. Moreover, hysteresis disappears at a very low oxygen concentration. This feature is important for understanding the mechanism of increasing ROS production at hypoxia-reoxygenation conditions. Our computational modeling results confirm a hypothesis [8] that hysteresis can underlie the mechanism of hypoxia-reoxygenation induced ROS generation in the entire respiratory chain during oxidation of NADH + succinate. We simulated in the model transient changes in the oxygen concentration $[O_2]$ from 2 to 0.02 μM with following returning $[O_2]$ from 0.02 to 2 μM under two different conditions, first, that mitochondrial membrane potential does not change, i.e. it is fixed at $\Delta\Psi = 160$ mV over transient changes in $[O_2]$ (Fig. 11,A and 11,B) and, second, $\Delta\Psi$ drops from 160 to 140 mV during decreasing $[O_2]$ from 2 to 0.02 μM (Fig. 11,C and 11,D). Results of computational simulation under fixed membrane potential at $\Delta\Psi = 160$ mV may be predicted from steady-state characteristics presented in Fig. 9,A and 9,B. For convenience, the value of $\Delta\Psi = 160$ mV is marked by a dashed vertical line in Fig. 9,A, so intersections of this vertical line and steady-state curves of the respiratory rate at

102

different oxygen concentration correspond to steady states at $\Delta\Psi = 160$ mV and $[O_2] = 2$, 0.2, 0.02, 0.002 μM, respectively. As Fig. 9,A and 9,B shows there are three steady-state values of the rate of respiration (Fig. 9,A) and superoxide production (Fig. 9,B) at $\Delta\Psi = 160$ mV and $[O_2] = 2$ μM, one of which (intermediate) is unstable and two others are stable. At the same time, only one steady state with a low respiration and a high ROS production remains at $\Delta\Psi = 60$ mV when $[O_2]$ decreases from 2 to 0.02 or 0.002 μM (blue dash-dot and green dash-dot-dot curves, respectively, in Fig. 9,A and 9,B). These features of steady-state characteristics determine a response in the rates of respiration and ROS production during transient changes in $[O_2]$ if the membrane potential keeps constant at $\Delta\Psi = 160$ mV.
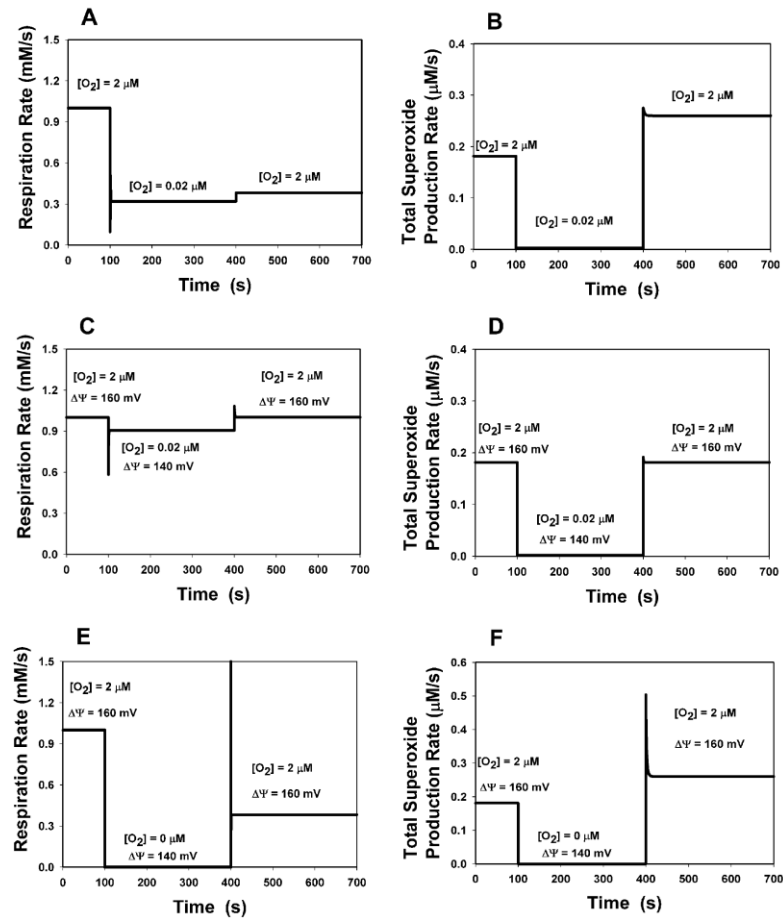

Figure 11. Computer simulation of hypoxia(anoxia)-reoxygenation. (**A–D**) Computer simulated transient switches in the rates of respiration (A, C) and total superoxide production (B, D) induced by temporal decreasing $[O_2]$ from 2 to 0.02 μM with returning $[O_2]$ from 0.02 to 2 μM. (**A, B**) Membrane potential was taken unchanged ($\Delta\Psi = 160$ mV) during the overall process of hypoxia-reoxygenation. (**C, D**) Membrane potential decreased from the initial value 160 mV to 140 mV during hypoxia (time interval 100–400 s) and returned to the initial value after reoxygenation at 400th s. (**E, F**) Computer simulated transient switches in the rates of respiration (**E**) and total superoxide production (**F**) induced by simultaneous temporal decreasing $[O_2]$ from 2 to 0 μM and $\Delta\Psi$ from 160 to 140 mV with returning $[O_2]$ from 0 to 2 μM and $\Delta\Psi$ from140 to 160 mV.

Fig. 11,A and 11,B presents computer simulation of transient changes in the rates of respiration (Fig. 11,A) and overall superoxide generation (Fig. 11,B) in the respiratory chain at $\Delta\Psi = 160$ mV during decreasing oxygen concentration $[O_2]$ from 2 to 0.02 μM with following returning $[O_2]$ from 0.02 to 2 μM. Initially during 100 s the respiratory chain is in the steady state with a high rate of respiration (Fig. 11,A) and a low rate of superoxide production (Fig. 11,B).

103

After decreasing $[O_2]$ from 2 to 0.02 μM at 100th s the respiratory chain switches to the steady state with low rates of respiration and superoxide production. After returning $[O_2]$ from 0.02 to 2 μM at 400th s the respiratory chain retains in the steady state with a low rate of respiration (Fig. 11,A), however, the superoxide production rate increases considerably and exceeds initial level at $[O_2] = 2$ μM (Fig. 8,B) due to more reduced state of electron carriers. Such scenario of alterations in the rates of respiration and ROS production is observed in the model during hypoxia-reoxygenation at a fixed value of $\Delta\Psi = 160$ mV.

However, *in vivo* the mitochondrial membrane potential may drop considerably upon inhibition of the respiratory chain during hypoxia. Therefore, consider another possible scenario when a decrease in $[O_2]$ from 2 to 0.02 μM is accompanied a decrease in the membrane potential, for example, from 160 to 140 mV. As Fig. 9 shows only one steady state with a high respiration and a low ROS production exists at $[O_2] = 0.02$ μM (blue dash-dot curves) and $\Delta\Psi = 140$ mV. This means that a decrease in the rate of respiration after decreasing $[O_2]$ from 2 to 0.02 μM is not so strong due to simultaneous decreasing $\Delta\Psi$ and the respiratory chain retains in the oxidized state after returning $[O_2]$ from 0.02 to 2 μM and $\Delta\Psi$ from 140 to 160 mV, i.e. the respiratory chain returns to the initial state with a high respiration and a low ROS production at $[O_2] = 2$ μM and $\Delta\Psi = 160$ mV after transient changes $[O_2]$ and $\Delta\Psi$. Direct numerical integration of the differential equations in the model confirms this conclusion. Fig. 11,C and 11,D presents computer simulated alterations in the rates of respiration (Fig. 11,C) and overall superoxide generation (Fig. 11,D) in the respiratory chain during simultaneous transient changes in $[O_2]$ and $\Delta\Psi$. Initially, just as in the previous case (Fig. 11,A and 11,B), during 100 s the respiratory chain is in the oxidized steady state with a high rate of respiration (Fig. 11,C) and a low rate of superoxide production (Fig. 11,D). After simultaneous decreasing $[O_2]$ from 2 to 0.02 μM and $\Delta\Psi$ from 160 to 140 mV at 100th s the respiratory chain transits to the steady state with a lower than initial but a high rate of respiration and a low rate of superoxide production, i.e. retains in the oxidized steady state. After simultaneous returning $[O_2]$ from 0.02 to 2 μM and $\Delta\Psi$ from 140 to 160 mV at 400th s the respiratory chain returns to the initial steady state with a high rate of respiration (Fig. 11,A) and a low rate of superoxide production (Fig. 11,D). This means that no changes occur in the steady-state ROS production rate compared to the initial state after reoxygenation following hypoxia if the membrane potential drops during hypoxia that keeping a high rate of respiration and oxidized steady state of the respiratory chain. However, the situation changes when not hypoxia but *anoxia* is accompanied a decrease in the membrane potential from 160 to 140 mV (Fig. 11,E and 11,F). After simultaneous decreasing $[O_2]$ from 2 to 0 μM and $\Delta\Psi$ from 160 to 140 mV at 100th s the respiratory chain transits to the steady state with the zero rates of respiration and superoxide production. In this case, the electron transport chain becomes reduced completely and after returning $[O_2]$ from 0 to 2 μM and $\Delta\Psi$ from 140 to 160 mV at 400th s the respiratory chain retains in the reduced steady state with a low rate of respiration (Fig. 11,E) and a high rate of superoxide production which exceeds an initial level at $[O_2] = 2$ μM (Fig.11,F) due to more reduced state of electron carriers.

Alterations in the mitochondrial membrane potential *in vivo* depend on the activity of numerous electrogenic transport systems in the inner mitochondrial membrane such as Ca^{2+}- and K^+-channels, adenine nucleotide translocase, electrogenic H^+ transport systems including H^+ leak and H^+ pumps of F_0F_1-ATPase and Complexes I, III and IV of the respiratory chain. Therefore, it would be expected a decrease in the membrane potential after inhibition of the respiratory chain and its H^+ pumps during hypoxia unless $\Delta\Psi$ keeps unchanged under special conditions.

Thus, our computational analysis shows that the mechanism based on bistability in the respiratory chain can account for an excess of ROS production during hypoxia-reoxygenation under condition only that the membrane potential keeps unchanged or depend a little bit on the

oxygen concentration. Otherwise, a drastic increase in ROS production resulted in ROS-related cellular hypoxia-reoxygenation injury [7] should be accounted for by additional alterations in mitochondria during hypoxia-reoxygenation.

3. Validation of modeling results by experimental data available in the literature

In order to validate quantitatively our computational modeling results on hysteresis and bistability in operation of the respiratory chain by experimental data available in the literature, we incorporated into the model additional equations describing explicitly changes in the electric potential of the inner mitochondrial membrane. Differential equation for changes in the membrane potential can be written as follows:

$$d(\Delta\Psi)\big/_{dt} = (4 \cdot v_{13} + v_{CIII} + 4 \cdot v_{40} - 3 \cdot v_{F1} - v_{Hle} - v_{Nle}) \cdot F / C, \tag{1}$$

where F is the Faraday constant and capacitance of inner membrane $C = 10^{-12}$ μM/mV [24].

In this equation, v_{13} and v_{40} represent outward transmembrane proton transport through Complexes I and IV, respectively. v_{CIII} represents a sum of fluxes of protons and electrons in Complex III. v_{F1} is inward H$^+$ flux through F1F0-ATP synthase, v_{Hle} and v_{Nle} are leakage fluxes of protons and non-specific ions, respectively, through the inner membrane.

Equation for v_{F1} was used following the work by Beard [24]:

$$v_{F1} = k_{F1} \cdot (\exp((-\Delta G_{0,ATP} + 3 \cdot \Delta G_H) / R \cdot T) \cdot ([ADP] \cdot [Pi] - 1M \cdot [ATP]), \tag{2}$$

$$\Delta G_{0,ATP} = -36.03 kJ / mol, \ \Delta G_H = F \cdot \Delta\Psi + R \cdot T \cdot \ln([H_0]/[H_i]), \ [H_0] = 0.1\mu M, [H_i] = 10^{-1.5}\mu M$$

Leakage fluxes are expressed as follows:

$$v_{Hle} = k_{Hle} \cdot (\exp(\Delta\Psi \cdot F / R \cdot T) \cdot ([H_0] - [H_i]) \tag{3}$$

$$v_{Nle} = k_{Nle} \cdot (\Delta\Psi - \Delta\Psi_{Nle}) \tag{4}$$

Electrogenic reactions of proton transport and electron transfer in Complex III relate to different parts of the inner membrane which are determined by location of Qo- and Qi-sites. Therefore, we took into account that the entire membrane potential $\Delta\Psi = \Delta\Psi_1 + \Delta\Psi_2 + \Delta\Psi_3$, where $\Delta\Psi_1$, $\Delta\Psi_2$ and $\Delta\Psi_3$ are portions of the membrane potential between: the Qi-site and mitochondrial matrix, the Qo- and Qi-sites, IMS and the Qo-site, respectively. Taking into account that $\Delta\Psi_1 = \delta_1 \cdot \Delta\Psi$, $\Delta\Psi_2 = \delta_2 \cdot \Delta\Psi$ and $\Delta\Psi_3 = \delta_3 \cdot \Delta\Psi$, where δ_1, δ_1 and δ_1 are dimensionless parameters describing in detail in Appendix, the summary rate of electrogenic reactions of proton transport and electron transfer in Complex III, i.e.

$$v_{CIII} = \delta_1 \cdot (v_{33} + v_{35}) + \delta_2 \cdot (v_{25} + v_{34}) + 2 \cdot \delta_3 \cdot v_{23} \tag{5}$$

In addition, validating our model by experimental data obtained by Selivanov and colleagues [8] we used their description of the rate of reduction of ubiquinone in Complex II that takes into account the succinate concentration, S:

$$v_1 = V_{\max 1} \cdot (Qn / (K_Q + Qn)) \cdot (S / (K_S + S)) \tag{6}$$

Our computer simulated results on the overall ROS production rate by the entire electron transport chain coincide with experimental observations by Selivanov and colleagues [8] of ROS production during oxidation of succinate alone (Fig. 12). Theoretical dependencies of the total ROS production rate (Fig. 12,A) and rates of superoxide generation by the semiqunone in

Complex I (Fig. 12,B) and the unstable semiquinone in Complex III (Fig. 12,C), as well as the respiratory rate (Fig. 12,D) on the succinate concentration have hysteresis shape with one unstable branch (dashed curves in each Figure) and two stable branches shown by solid curves. The steady-state rate of superoxide generation by the reduced flavin in Complex I not shown because it is very small compared to the ROS production rates by semiquinones in Complex I and III during oxidation of succinate alone. Experimental data on the ROS production rate shown in Fig. 12,A by triangles and squares are reproduced from Fig. 4,B of the work by Selivanov and colleagues [8]. Original experimental data were represented in [8] as the dimensionless relative ROS production rate. In order to fit these data to our computer simulated results they were multiplied by factor 2 μM/s. A break in Fig. 12,A was introduced for more extended presentation of the portion of the theoretical curve corresponding to experimental data.
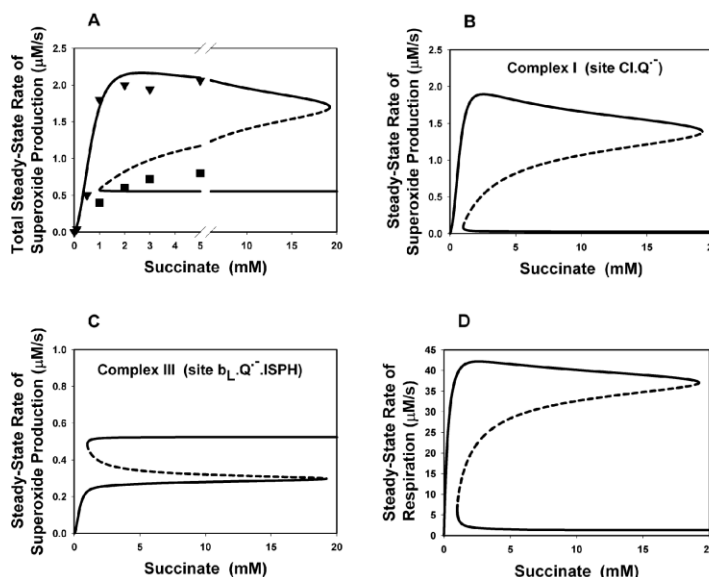

Figure 12. Computer simulated and experimentally observed bistable dependence of rates of respiration and ROS production on the succinate concentration. (**A**) Comparison of computational modeling results (lines) and experimental data (symbols) on overall ROS production in the electron transport chain. Experimental data were reproduced from [8]. (**B, C**) Dependence of computer simulated rates of superoxide generation by the semiquinones of Complex I (**B**) and III (**C**) on the succinate concentration. (**D**) Dependence of the computer simulated rate of respiration on the succinate concentration. Solid lines correspond to stable steady states in the computational model, dashed lines-unstable steady states. Computer simulation was carried out at kinetic parameter values presented in Table 2 in [13] except $k_8 = 100$ μM^{-1}s^{-1}; $K_{eq8} = 0.01$ μM^{-1}; $K_{eq14} = 10^3$ μM^{-1}; $k_{22} = 5 \cdot 10^{-6}$ μM^{-2}s^{-1}; $K_{eq22} = 1 \cdot 10^{-4}$ μM^{-2}; $K_{eq23} = 10$; $K_{eq26} = 1 \cdot 10^5$ μM; $k_{28} = k_{29} = 6$ μM^{-1}s^{-1}; $k_{32} = 0.008$ μM^{-1}s^{-1}; $k_{36} = 1000$ s^{-1}; $K_{eq36} = 1 \cdot 10^5$ μM; $k_{F1} = 1 \cdot 10^{-18}$ μM^{-1}s^{-1}; [ATP] $= 5 \cdot 10^3$ μM; [Pi] $= 1 \cdot 10^4$ μM; [ADP] $= 0$; [Ho] $= 0.1$ μM, [Hi] $= 1 \cdot 10^{-1.5}$ μM; $V_{max1} = 300$ μM/s; $K_Q = 100$ μM; $K_s = 0.5$ mM; $k_{Hle} = 8$ s^{-1}; $k_{Nle} = 10$ μM s^{-1} · mV^{-1}; $\Delta\Psi_{Nle} = 175$ mV.

The most important feature of the theoretical results presented in Fig. 12 is the following. The rate of superoxide generation by the semiqunone in Complex I (Fig. 12,B) follows the respiratory rate (Fig. 12,D), i.e. the stable branch with a high rate of ROS production by this semiqunone corresponds to a high rate of respiration and, consequently, to the oxidized state of the electron transport chain. And the less rate of respiration, i.e. the more reduced state of the respiratory chain, induces less superoxide generation by the semiqunone in Complex I (Fig. 12,B). This theoretical prediction which contradicts an opinion that the more reduced electron transport chain generates the more superoxide can be accounted for a high sensitivity of concentration of the semiqunone in Complex I to the oxidized qunone, Q, which located upstream of this semiqunone

106

as shown in the kinetic scheme in Fig. 1 (Qn in reaction 8). A high respiration rate results in a more generation of Q in Complex III and more concentration of the semiqunone in Complex I and the rate of superoxide generation by this semiqunone, respectively. On the contrary, the ROS production rate by the unstable semiquinone in Complex III (Fig. 12,C) is much more sensitive to quinol, QH2p, located upstream of the unstable semiquinone (reaction 22 in Fig. 1). This means that the ROS production rate in Complex III is a higher under the reduced state of the electron transport chain, i.e. a high stable branch of superoxide generation by the unstable semiquinone in Complex III (Fig. 12,C) corresponds to a low respiration rate (Fig. 12,D). The maximal rate of ROS generation by the semiqunone in Complex I (Fig. 12,B) is higher than by the unstable semiquinone in Complex III (Fig. 12,C) during oxidation of succinate alone. Therefore, the overall rate of ROS production by the electron transport chain during oxidation of succinate alone follows the rate of respiration as ROS generation by the semiqunone in Complex I does.

Other important physiological conclusion from our computer modeling results is the following. The opposite dependence of bistable switches in ROS production by the semiquinones of Complexes I and III on the respiration rate gives a possibility to control bistable switches in ROS production in moderate physiological range during bistable switches in the respiration rate. Really, a bistable switch from the steady state with a high to a low respiration rate results in a transition in the ROS production from Complex III to Complex I. This allows to prevent the electron transport chain from excessive ROS generation and, in other hand, to keep overall ROS production at the level sufficient for physiological needs.

CONCLUSION

1. Hysteresis and bistability in respiratory chain operation during oxidation of NADH and succinate has the same kinetic mechanism, namely an apparent substrate inhibition of QH$_2$ oxidation at the Qo-site of Complex III

It is well known that hysteresis and bistability can arise from product activation or substrate inhibition in metabolic pathways [15] and multisite phosphorylation in signaling pathways [25]. The mechanism by which bistability arises in the respiratory chain has another origin and results from the specific features of the Q-cycle, in which the Qo- and Qi-site compete for the substrate ubiquinone due to total intramembrane ubiquinone conservation as was noticed earlier by Selivanov and colleagues [8]. An increase in ubiquinol QH$_2$, the substrate for the Qo-site, results automatically in a decrease in oxidized ubiquinone Q, the substrate for the Qi-site, due to total Q conservation. As a result, a reduction of Q at the Qi-site is inhibited upon increasing QH$_2$, resulting in a break in the Q-cycle and inhibition of reactions at the Qo-site at the steady state. In turn, increasing Q results in a decrease in QH$_2$ and inhibition of the Qo-site reactions, also breaking the Q-cycle and inhibiting reduction of Q at the Qi-site. Thus, a dependence of reactions at the Qo- and Qi-site on substrates QH$_2$ and Q, respectively, has a bell-shaped form (Fig. 3, 4) similar to reactions with substrate inhibition, which can result in bistability in their operation [16]. These specific features are the main reason for the Q-cycle and all respiratory chain to function as a trigger switching between two stable states with low and high rates of respiration and ROS production as well as reduced and oxidized states of ubiquinone and Fe-S clusters of Complex I during NADH + succinate oxidation (Fig. 2).

2. Hypoxia-reoxigenation can increase ROS production considerably

Bistability in the respiratory chain relates to trigger switches in the ROS production rate during changes in the metabolic state of mitochondria, which is very important for mitochondrial physiology. The most dramatic bistable switches in mitochondrial ROS production can occur

during changes in the oxygen concentration which result in two simultaneous events, first, bistable switches in the redox state of the respiratory chain and, second, changes in the substrate concentration for superoxide generation. Considerable changes in ROS production during hypoxia-reoxigenation (Fig. 11,A and 11,B) is one of such examples. Therefore, it is very important to know a region of existence of bistability in the respiratory chain and can control it. However, a computational simulation of hypoxia-reoxygentaion with numerical integration of the model under bistability condition shows a considerable increase in the rate of ROS production under condition only that hypoxia and accompanying decrease in the membrane potential induce a transition of the respiratory chain to the oxidized steady state.

3. A comparison of our explicit network computational model to the Selivanov's rule-based model of the respiratory chain

Our computational analysis shows that computer simulated results on ROS production in the respiratory chain from our explicit network computational model and the rule-based model developed recently by Selivanov and colleagues [8, 9] are very similar. First of all, it is related to common kinetic features of the respiratory chain and, in particular, availability of bistability in operation of Complex III, e.g. the Mitchel's Q-cycle, and a possible considerable increase in ROS production during hypoxia-reoxygenation related to this bistability. However, some features on ROS production in antimycin-inhibited Complex III [11, 12] can be attributed to the explicit network computational model only because they can be accounted for at the assumption only that the rate constants of oxidation of ISPH and QH_2 at the Qo-site strongly depend on the redox state of cyt b.

TESTABLE PREDICTIONS

Our computer simulated results predict hysteresis and bistability in the respiratory chain during oxidation of NADH alone and NADH + succinate. This means that the rates of respiration and ROS production, as well as the redox states of Fe-S clusters N3, N1b, N4, N5, N6a, N6b, and N2 of Complex I and the concentration of oxidized/reduced ubiquinone can switch between two alternative stable states during changes in the membrane potential. The most favorable values of the membrane potential for bistability to arise are in the range of 100–170 mV (Fig. 2–8). The most important factors which affect occurrence of bistability in the respiratory chain and can be controlled experimentally are the rates of. NADH reduction in the matrix and the total concentration of Complex I [CI] and ubiquinone $[Q]_{tot}$ in the inner membrane (Fig. 2, 7, 8). A high rate of NADH reduction and a high ratio [CI]/ $[Q]_{tot}$ are condition that would favorable for hysteresis and bistability.

Acknowledgements

APPENDIX.
COMPUTATIONAL ANALYSIS OF HYSTERESIS AND BISTABILITY IN THE MITOCHONDRIAL RESPIRATORY CHAIN

The basic mathematical model consists of a system of 32 ordinary differential equations (ODE) according to chemical equations presented in Table 1 and parameter values in Table 2 presented in our previous work [13] and 12 moiety conservations equations.

Differential equations

$F[1] = d[\text{QH2p}]/dt = 2 \cdot (v_{20} - v_{22})$

$F[2] = d[\text{QH2n}]/dt = v_{19} - 2 \cdot v_{20} + v_{36} + v_{14}$

$F[3] = d[\text{Qp}]/dt = 2 \cdot (v_{26} - v_{21})$

$F[4] = d[\text{bL.QH2p.ISP}]/dt = 2 \cdot (v_{22} - v_{23})$

$F[5] = d[\text{bL.Q}^{\cdot-}.\text{ISPH}]/dt = 2 \cdot (v_{23} - v_{24} - v_{28} - v_{29})$

$F[6] = d[\text{bL}^{-}.\text{Q}]/dt = 2 \cdot v_{24} - v_{25} - v_{34}$

$F[7] = d[\text{bL.Q}]/dt = v_{25} + v_{34} - 2 \cdot v_{26} + 2 \cdot v_{28} + 2 \cdot v_{29}$

$F[8] = d[\text{ISPH}]/dt = 2 \cdot (v_{24} - v_{27})$

$F[9] = d[\text{bH}^{-}]/dt = v_{25} - v_{32}$

$F[10] = d[\text{bH}^{-}.\text{Qn}]/dt = v_{32} - v_{33}$

$F[11] = d[\text{bH.QH}]/dt = v_{33} - v_{34}$

$F[12] = d[\text{bH}^{-}.\text{QH}]/dt = v_{34} - v_{35}$

$F[13] = d[\text{bH.QH}_2]/dt = v_{35} - v_{36}$

$F[14] = d[\text{c1}^{-}]/dt = 2 \cdot (v_{27} - v_{37})$

$F[15] = d[\text{c1}^{\cdot}.\text{c}]/dt = 2 \cdot (v_{37} - v_{38})$

$F[16] = d[\text{c1.c}^{-}]/dt = 2 \cdot (v_{38} - v_{39})$

$F[17] = d[\text{c}^{-}]/dt = 2 \cdot (v_{39} \cdot \textit{Wimb/Wims} + v_{31} - v_{40} \cdot \textit{Wimb/Wims})$

$F[18] = d[\text{O}_2^{\cdot-}{}_{IMS}]/dt = 2 \cdot (v_{28} \cdot \textit{Wimb/Wims} - 2 \cdot v_{30} - v_{31})$

$F[19] = d[\text{FMN.NAD}]/dt = v_4$

$F[20] = d[\text{NADH}]/dt = -v_1 \cdot \textit{Wimb/Wmx} - v_5 \cdot \textit{Wimb/Wmx} + v_{15}$

$F[21] = d[\text{FMNH}^{-}.\text{NADH}]/dt = v_5$

$F[22] = d[\text{FMN.NADH}]/dt = v_1 - v_2$

$F[23] = d[\text{FMNH}^{-}.\text{NAD}]/dt = v_2 - v_3$

$F[24] = d[\text{FMNH}^{-}]/dt = v_3 - v_5 - v_6 - v_{16}$

$F[25] = d[\text{FMNH}^{\cdot}]/dt = v_{16} + v_6 - v_{10} - v_{11}$

$F[26] = d[\text{N3}^{-}]/dt = v_6 - v_7 + v_{11} - v_{12}$

$F[27] = d[\text{N2}^{-}]/dt = v_7 + v_{12} - v_9 - v_{13}$

$F[28] = d[\text{N1a}^{-}]/dt = v_{10}$

$F[29] = d[\text{CI.Q}]/dt = v_8 - v_9 + v_{17}$

$F[30] = d[\text{CI.Q}^{\cdot-}]/dt = v_9 - v_{13} - v_{17}$

$F[31] = d[\text{CI.QH2}]/dt = v_{13} - v_{14}$

$F[32] = d[\text{O}_2^{\cdot-}{}_{mx}]/dt = (v_{16} + v_{17} + v_{29}) \cdot \textit{Wimb/Wmx} - 2 \cdot v_{18}$

Moiety conservations equations

$\text{NAD} = \text{NAD}_{tot} - (\text{FMN.NAD} + \text{NADH} + \text{FMN.NADH} + \text{FMNH}^{-}.\text{NAD} + \text{FMNH}^{-}.\text{NADH})$

$\text{FMN} = \text{FMN}_{tot} - (\text{FMN.NAD} + \text{FMN.NADH} + \text{FMNH}^{-}.\text{NAD} + \text{FMNH}^{-}.\text{NADH} + \text{FMNH}^{-} + \text{FMNH}^{\cdot})$

$\text{N1a} = \text{N1a}_{tot} - \text{N1a}^{-}$

$\text{N2} = \text{N2}_{tot} - \text{N2}^{-}$

$N3 = N3_{tot} - N3^-$

$CI = CI_{tot} - (CI.Q + CI.Q^{\cdot -} + CI.QH2)$

$Qn = Q_{tot} - (QH2n + Qp + QH2p + bL.QH2p.ISP + bL.Q^{\cdot -}.ISPH + bL^-.Q.ISPH + bL.Q.ISPH + bH^-.Qn + bH.QH + bH^-.QH + bH.QH2 + CI.Q + CI.Q^{\cdot -} + CI.QH2)$

$bL = bL_{tot} - (bL^- + bL.QH2p.ISP + bL.Q^{\cdot -}.ISPH + bL^-.Q.ISPH + bL.Q.ISPH)$

$bH = bH_{tot} - (bH^- + bH^-.Qn + bH.QH + bH^-.QH + bH.QH2)$

$ISP = ISP_{tot} - (bL.QH2p.ISP + bL.Q^{\cdot -}.ISPH + ISPH)$

$c1 = c1_{tot} - (c1^- + c1^-.c + c1.c^-)$

$c = c_{tot} - (c^- + Vim/Vims \cdot (c1^-.c + c1.c^-))$

REFERENCES

1. Droge W. *Physiol. Rev*. 2002. V. 82. P. 47–95.
2. Barja G. *Trends Neurosci*. 2004. V. 27. P. 595–600.
3. Balaban R.S., Nemoto S., Finkel T. *Cell*. 2005. V. 120. P. 483–495.
4. Andreyev A.Y., Kushnareva Y.E., Starkov A.A. *Biochemistry*. 2005. V. 70. P. 200–214.
5. Murphy M.P. *Biochem. J*. 2009. V. 417. P. 1–13.
6. Bailey S.M., Cunningham C.C. *Free. Radic. Biol. Med*. 2002. V. 32. P. 11–16.
7. Li C., Jackson R.M. *Am. J. Physiol. Cell. Physiol*. 2002. V. 282. P. C227–C241.
8. Selivanov V.A., Votyakova T.V., Zeak J.A., Trucco M., Roca J., Cascante M. *PLoS Comput. Biol.* 2009. V. 5. P. e1000619.
9. Selivanov V.A., Votyakova T.V., Pivtoraiko V.N., Zeak J., Sukhomlin T., Trucco M., Roca J., Cascante M. *PLoS Comput. Biol*. 2011. V. 7. P. e1001115.
10. Borisov N.M., Markevich N.I., Hoek J.B., Kholodenko B.N. *Biophys. J*. 2005. V. 89. P. 951–966.
11. Yu C.A., Cen X., Ma H.W., Yin Y., Yu L., Esser L., Xia D. *Biochim. Biophys. Acta.* 2008. V. 1777. P. 1038–1043.
12. Quinlan C.L., Gerencser A.A., Treberg J.R., Brand M.D. *J. Biol. Chem.* 2011. V. 286. P. 31361–31372.
13. Markevich N.I., Hoek J.B. *Mathematical Biology and Bioinformatics*. 2014. V. 9. № 1. P. 63-88.
14. Batandier C., Guigas B., Detaille D., El-Mir M.Y., Fontaine E., Rigoulet M., Leverve X.M. *J. Bioenerg. Biomembr.* 2006. V. 38. P. 33–42.
15. Hirst J., King M.S., Pryde K.R. *Biochem. Soc. Trans*. 2008. V. 36. P. 976–980.
16. Sel'kov E.E. *Eur. J. Biochem.* 1975. V. 59. P. 151–157.
17. Vinogradov A.D. *Biochim. Biophys. Acta.* 1998. V. 1364. P. 169–185.
18. Moser C.C., Farid T.A., Chobot S.E., Dutton P.L. *Biochim. Biophys. Acta.* 2006. V. 1757. P. 1096–1109.
19. Verkhovskaya M.L., Belevich N., Euro L., Wikstrom M., Verkhovsky M.I. *Proc. Natl. Acad. Sci. U S A.* 2008. V. 105. P. 3763–3767.
20. Grivennikova V.G., Vinogradov A.D. *Biochim. Biophys. Acta*. 1982. V. 682. P. 491–495.
21. Clanton T. *J. Appl. Physiol.* 2005. V. 99. P. 1245–1246.
22. Guzy R.D., Schumacker P.T. *Exp. Physiol*. 2006. V. 91. P. 807–819.
23. Hoffman D.L., Brookes P.S. *J. Biol. Chem.* 2009. V. 284. P. 16236–16245.
24. Beard D.A. *PLoS Comput. Biol*. 2005. V. 1. P. e36.
25. Markevich N.I., Hoek J.B., Kholodenko B.N. *J. Cell. Biol.* 2004. V. 164. P. 353–359.